Article

Poly(vinylpyrrolidone)-Modified Graphite Carbon Nanofibers as Promising Supports for PtRu Catalysts in Direct Methanol Fuel Cells

Yu Lin Hsin, Kuo Chu Hwang, and Chuin-Tih Yeh

J. Am. Chem. Soc., **2007**, 129 (32), 9999-10010• DOI: 10.1021/ja072367a • Publication Date (Web): 21 July 2007

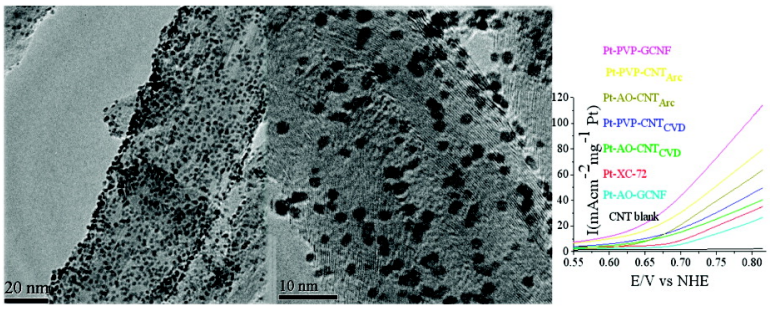

More About This Article

Additional resources and features associated with this article are available within the HTML version:

- Supporting Information
- Links to the 7 articles that cite this article, as of the time of this article download
- Access to high resolution figures
- Links to articles and content related to this article
- Copyright permission to reproduce figures and/or text from this article

View the Full Text HTML

J|A|C|S
ARTICLES
Published on Web 07/21/2007

Poly(vinylpyrrolidone)-Modified Graphite Carbon Nanofibers as Promising Supports for PtRu Catalysts in Direct Methanol Fuel Cells

Yu Lin Hsin, Kuo Chu Hwang,* and Chuin-Tih Yeh

Contribution from the Department of Chemistry, National Tsing Hua University, Hsinchu, Taiwan

Received April 13, 2007; E-mail: kchwang@mx.nthu.edu.tw

Abstract: Carbon nanomaterials, including herringbone graphite carbon nanofibers (GNF_H), multiwalled carbon nanotubes (MWCNT), and carbon black, were surface-modified by a new poly(vinylpyrrolidone) (PVP) grafting process as well as by the conventional acid-oxidation (AO) process, and characterized by FTIR, TGA, Raman, HRTEM, XRD, and XPS measurements. Pt nanoparticles of 1.8 nm were evenly deposited on all PVP-grafted carbon nanomaterials. The effects of the two surface modification processes on the dispersion, average Pt nanoparticle sizes, the electrocatalytic performance, and electrical conductivities of Pt−carbon nanocomposites in direct methanol oxidation were systematically studied and compared. It was found that the PVP-grafted carbon nanomaterials have much less loss in the electric conductivity and thus better electrocatalytic performance, 17−463% higher, than their corresponding acid oxidation-treated nanocomposites. The electrocatalytic performance of the Pt−carbon nanocomposites decreases in the following order: Pt−PVP−GNF_H > Pt−PVP−$MWCNT_{arc}$ > Pt−AO-$MWCNT_{arc}$ > Pt−PVP−$MWCNT_{CVD}$ > Pt−AO-$MWCNT_{CVD}$ > Pt−XC-72R > Pt−AO-GNF_H, with the Pt−PVP−GNF_H nanocomposite having ∼270% higher performance than that of the Pt−Vulcan XC-72R nanocomposite. In addition, PtRu−PVP−GNF_H shows even better (50% higher) electrocatalytic activity than the Pt−PVP−GNF_H nanocomposite at a 0.6 V applied voltage.

Introduction

The investigation of fuel cells in searching for high efficiencies and high capacities has attracted a lot of attention in recent years[1−3] because of the fast development of and large power requirements for portable electronic devices, such as, personal digital assistants (PDAs), cell phones, notebook personal computers, etc. The direct methanol fuel cell (DMFC) is especially attractive since it operates at room temperature, uses liquid methanol as the fuel, and eliminates the expensive setup of hydrogen reformers and the hydrogen storage problem. In DMFC, the metal catalysts for direct methanol oxidation are usually Pt or PtRu nanoparticles deposited on carbon nanosupports.[4−21] The performance of a DMFC is strongly affected by many factors, such as the sizes, the amount, and the dispersion of the catalyst nanoparticles and the total surface area of carbon supports. To reduce the cost of DMFC, the total amount of expensive noble metal catalysts loaded on carbon supports has to be reduced, but the electrochemically active surface (EAS) area of metal catalysts and the overall performance of fuel cells have to remain unchanged or higher. For a given amount (or weight) of metal catalysts, the smaller the size of metal nanoparticles is, the larger the EAS will be. To this end, the average size of metal nanoparticle catalysts has to be reduced as much as possible and aggregation of metal nanoparticles avoided by using carbon supports of large surface area, such as Vulcan XC-72R carbon black (surface area ∼250 $m^2\ g^{-1}$). Many other carbon nanomaterials, such as graphite carbon nanofibers

(1) Appleby, A. J.; Foulkes, F. R. In *Fuel Cell Handbook*; Van Nostrand Reinhold: New York.
(2) Serp, P.; Corrias, M.; Kalck, P. *Appl. Catal. A. Gen.* **2003**, *253*, 337.
(3) Liu, H.; Song, C.; Zhang, L.; Zhang, J.; Wang, H.; Wilkinson, D. P. *J. Power Sources* **2006**, *155*, 95.
(4) Steigerwalt, E. S.; Deluga, G. A.; Lukehart, C. M. *J. Phys. Chem. B* **2002**, *106*, 760.
(5) Girishkumar, G.; Hall, T. D.; Vinodgopal, K.; Kamat, P. V. *J. Phys. Chem. B* **2006**, *110*, 107.
(6) Matsumoto, M.; Komatsu, T.; Arai, K.; Yamazaki, T.; Kijima, M.; Shimizu, H.; Takasawa, Y.; Nakamura, J. *Chem. Commun.* **2004**, 840.
(7) Gu, Y. J.; Wong, W. T. *Langmuir* **2006**, *22*, 11447.
(8) Liao, S.; Holmes, K. A.; Taprailis, H.; Birss, V. I. *J. Am. Chem. Soc.* **2006**, *128*, 3504.
(9) Prabhuram, J.; Zhao, T. S.; Tnag, Z. K.; Chen, R.; Liang, Z. X. *J. Phys. Chem. B* **2006**, *110*, 5245.
(10) Hyeon, T.; Han, S.; Sung, Y. E.; Park, K. W.; Kim, Y. W. *Angew. Chem., Int. Ed.* **2003**, *42*, 4352.
(11) Bessel, C. A.; Laubernds, K.; Rodriguez, N. M.; Baker, R. T. K. *J. Phys. Chem. B* **2001**, *105*, 1115.
(12) Che, G.; Lakshmi, B. B.; Martin, C. R.; Fisher, E. R. *Langmuir* **1999**, *15*, 750.
(13) Yu, R. Q.; Chen, L. W.; Liu, Q. P.; Lin, J. Y.; Tan, K. L.; Ng, S. C.; Chan, H.; Xu, G. Q.; Andyhor, T. S. *Chem. Mater.* **1998**, *10*, 718.
(14) Kim, Y. -T.; Mitani, T. *J. Catal.* **2006**, *238*, 394.
(15) Li, W.; Wang, X.; Chen, Z.; Waje, M.; Yan, Y. *J. Phys. Chem. B* **2006**, *110*, 15353.
(16) Kim, C.; Kim, Y. J.; Kim, Y. A.; Yanagisawa, T.; Park, K. C.; Endo, M.; Dresselhaus, M. S. *J. Appl. Phys.* **2004**, *96*, 59030.
(17) Li, W.; Liang, C.; Qiu, J.; Zhou, W.; Han, H.; Wei, Z.; Sun, G.; Xin, Q. *Carbon* **2002**, *40*, 787.
(18) Toebes, M. L.; van der Lee, M. K.; Tang, L. M.; Huis in't Veld, M. H.; Bitter, J. H.; Jos van Dillen, A.; de Jong, K. P. *J. Phys. Chem. B* **2004**, *108*, 11611.
(19) Li, W.-Z.; Liang, C.-G.; Zhou, W.-J.; Qiu, J.-S.; Zhou, Z.-H.; Sun, G.-Q.; Xin, Q. *J. Phys. Chem. B* **2003**, *107*, 6292.
(20) Huang, S.-Y.; Chang, S.-M.; Yeh, C.-T. *J. Phys. Chem. B* **2006**, *110*, 234.
(21) Tian, Z. Q.; Jiang, S. P.; Liang, Y. M.; Shen, P. K. *J. Phys. Chem. B* **2006**, *110*, 5343.

(GNF),[4] single-walled carbon nanotubes (SWCNT),[5] multiwalled carbon nanotubes (MWCNT),[6−9] and carbon nanocoils,[10] were also investigated for the use as anodic supports in DMFC. Without surface modification, it was reported that Pt metal catalyst deposited on GNF (with a narrow herringbone structure) gives a better performance than those deposited on SWCNT and MWCNT, and has 64% increase in the cell performance as compared to that of unsupported catalyst colloids.[4] However, the mean size of Pt nanoparticles in these surface-unmodified carbon supports is quite large, in the range of 5.8−12.6 nm. It was also reported that the electrocatalytic performance of a 5 wt % Pt nanoparticles (with sizes of 2−10 nm) deposited on surface unmodified "ribbon" and "platelet" GNF is comparable to that of 25 wt % loading of Pt on Vulcan XC-72R carbon black.[11] A Pt−MWCNT nanocomposite was reported to have 20 times higher performance than that of bulk Pt electrode.[12] Without surface modification, most of carbon nanomaterials lack sufficient binding sites for anchoring precursor metal ions or metal nanoparticles, which usually leads to poor dispersion and aggregation of metal nanoparticles, especially at high loading conditions. To introduce more binding sites and surface anchoring groups, an acid oxidation process was very frequently adopted to treat carbon nanomaterials in a refluxed, mixed acid aqueous solution at high temperatures (90−140 °C), which introduces surface-bound polar hydroxyl and carboxylic acid groups for subsequent anchoring and reductive conversion of precursor metal ions to metal nanoparticles in the presence of ethylene glycol.[13] Besides the surface carboxylic acid groups, thiol groups could also be introduced onto CNT graphene walls via amide bond formation between surface carboxylic acid groups and $NH_2C_6H_4SH$.[14] It was reported that PtRu alloy nanoparticles of 2−3 nm in diameter could be successfully deposited onto double-walled carbon nanotubes (DWCNT), SWCNT, and MWCNT via the acid oxidation−ethylene glycol reduction process.[15] The electrocatalytic performance of the PtRu−AO-DWCNT nanocomposite on direct methanol oxidation was reported to have 68% enhancement in the power density as compared to that of PtRu−E-TEK carbon black nanocomposite. It was also reported that PtRu alloy nanoparticles with an average size of 5.0−6.5 nm can be well dispersed on acid-oxidized cap-stacked carbon nanotubes (AO-CSCNT).[16] The PtRu−AO-CSCNT nanocomposite could provide nearly 2-fold higher power density than that for a PtRu−Vulcan XC-72R carbon black nanocomposite. A PtRu−AO-MWCNT nanocomposite with 3−4 nm PtRu nanoparticles was reported to have 35−39% higher DMFC electrocatalytic performance than that for a PtRu−Vulcan XC-72R nanocomposite,[9] which is in very sharp contrast to another report of a Pt−AO-MWCNT nanocomposite having a 5-fold better DMFC performance than that for a Pt−Vulcan XC-72 R nanocomposite.[17] M. L. Toebes et al.[18] have successfully prepared a Pt−AO-GNF nanocomposite with a very small Pt nanoparticle size of 1−2 nm but did not report the DMFC electrocatalytic performance. Pt−nanocomposites using MWCNT as carbon supports have frequently been reported to have better DMFC electrocatalytic performance than those for Vulcan XC-72R carbon black as supports, despite the average surface area of MWCNT (ranging from 20−60 m^2g^{-1})[21] being far less than that (∼250 $m^2\ g^{-1}$) of the Vulcan XC-72R carbon black. Many researchers have attributed the superior performance of MWCNT to their good electrical conductivities.[16,17,19,21] However, direct measurements of electric conductivities of various carbon nanomaterials are still lacking.

In general, surface functionalization of carbon supports could increase the surface binding sites, avoid the formation of metal aggregates, improve the dispersion of metal nanoparticles, and reduce the average size of metal nanoparticles deposited but is also inevitably accompanied with a few problems, such as uneven distribution of the surface functional groups, structural damage, and thus partial loss in electrical conductivity of the carbon supports. The surface functional groups (e.g., carboxyl, hydroxyl, carbonyl groups) on the acid-oxidized carbon nanomaterials are mostly concentrated at defects sites or at the end tips (in the case of CNT), where the strain and/or the chemical reactivity are higher. Prolonged acid oxidation at higher temperatures could lead to CNT end cap opening[22,23] and more oxidative damage on graphene structures, leading to potentially more severe loss in the electric conductivity of carbon nanomaterials. To minimize the above disadvantages, it is highly desirable to develop a mild surface functionalization process to introduce high density and homogeneous surface functional groups but cause limited structural damage to the carbon nanomaterials (and thus retain good electrical conductivity).

In this study, we have (a) developed a new PVP surface modification process in aqueous solutions, which is able to introduce high density and homogeneous surface functional groups on various carbon nanomaterials. (b) Many carbon nanomaterials, including herringbone graphite carbon nanofibers, multiwalled carbon nanotubes from arc discharge ($MWCNT_{arc}$) or from chemical vapor deposition ($MWCNT_{CVD}$), and commercial carbon blacks (Vulcan XC-72R), were surface functionalized by PVP grafting as well as the acid oxidation processes, and well characterized by various spectroscopic measurements, including FTIR, thermal gravity analysis (TGA), HRTEM, Raman, XRD, and XPS. (c) Our electric conductivity measurements show that the PVP grafting process causes much less loss in the electric conductivity of carbon nanomaterials than that for the conventional acid oxidation method. In the case of GNF_H, 51% electric conductivity was retained for the PVP−GNF_H but is only 10% for the AO-GNF_H. (d) Pt nanoparticles of 1.8 nm were evenly deposited on these PVP-grafted carbon nanomaterials. The electrocatalytic performance of all Pt−PVP−carbon nanocomposites on the direct oxidation of methanol was systematically studied and compared with those of the same carbon nanomaterials treated by the conventional acid oxidation method. (e) It was found that Pt−PVP−carbon nanocomposites have 17−463% higher activity than that for the corresponding Pt−carbon nanomaterials treated by acid oxidation. PVP-modified herringbone graphite carbon nanofiber shows the highest performance among all the carbon nanomaterials investigated in this study and has about 270% higher performance than that of Pt−Vulcan XC-72R nanocomposite. (f) A PtRu−PVP−GNF_H nanocomposite was also prepared, of which the electrocatalytic activity is ∼50% higher than that of the Pt−PVP−GNF_H nanocomposite at an applied voltage of 0.6 V.

Experimental Section

Preparation of Carbon Supports. MWCNT were produced by a two-step chemical vapor deposition (CVD) method as described in the literature.[24] Briefly, MWCNT were grown on a quartz glass by injection (4 mL/h) of a ferrocene (5 wt/wt %)−toluene solution into the first

Scheme 1. Schematic View of Attachment of Poly(vinylpyrrolidone) Moieties on Carbon Nanomaterials

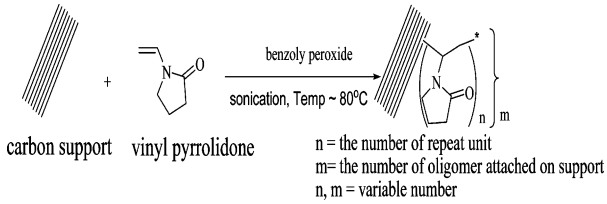

stage of a furnace at 200 °C under an argon flow of 200 sccm. The ferrocene−toluene vapor was then swept into the second stage furnace to have thermal pyrolysis at 900 °C where the vertically aligned nanotube films were grown from both flat quartz substrates and the surrounding reaction chamber. The MWCNT solid film was collected and ground into powder form by high-speed zirconium oxide ball milling for 24 h. The grinding process splits large aligned MWCNT bundles into small pieces from which the amorphous carbon and metal particles can be easily removed by refluxing a short time in an acid (concentrated $HNO_3-H_2SO_4$ in 1:1 v/v ratio) solution at 90 °C for 30 min. The short time acid treatment is not expected to cause severe structural damage or surface functionalization on MWCNT. The purified MWCNT were labeled as $MWCNT_{CVD}$. MWCNT produced from an arc-discharge method[25] were purified by the same short time acid treatment process and labeled as $MWCNT_{arc}$. The $MWCNT_{arc}$ with diameters in the range of 4−60 nm have hollow, well-graphitized multiple walls graphene layer structures. Herringbone graphite carbon nanofibers (GNF_H) with 20−40 nm diameters and purity of 95% were purchased from Shenzhen Nanotech Port Co., Ltd, China. The GNF_H were purified by heating a short time in a 4 N HNO_3 at 70 °C for 30 min. Commercial carbon black (Vulcan XC-72R; surface area: 250 m^2g^{-1}) was also used as metal catalyst supports (without any further surface modification) for the purpose of comparison.

Surface area measurements of the carbon supports were preformed volumetrically in a vacuum system at a bath temperature of 77 K using nitrogen gas as the adsorbate. Surface areas were obtained using the Brunauer−Emmett−Teller (BET) equation to fit the experimental data. For nitrogen physisorption, about 0.2 g sample was inserted into an adsorption cell connected to a volumetric system. Prior to the measurement, each sample was pretreated with an evacuation at 10^{-6} Pa at 473 K for 4 h in the sample cell. The increment of nitrogen uptake was calculated from the pressure change of the system, which was monitored by a Texas pressure gauge (with a resolution of 1 Pa).

Surface Modification of Carbon Nanomaterials. Acid oxidation of MWCNT was accomplished by following a literature procedure, i.e., refluxing MWCNT a long time in a mixed acid (H_2SO_4:HNO_3 in 1:1 v/v ratio) solution at 140 °C for 4 h. The procedure for surface modification of carbon nanomaterials with poly(vinylpyrrolidone) is similar to our previously reported procedure[26] and is schematically presented in Scheme 1. Briefly, 300 mg of carbon nanomaterials was suspended in 10 mL of liquid vinylpyrrolidone containing 100 mg of benzoyl peroxide. The mixture was ultrasonicated in a cup type ultrasonicator (Heat system Inc., XL-2020, 550 W, 20 kHz) for 10 min, and the solution temperature usually reached ~80 °C. Then, another 100 mg of benzoyl peroxide was added into the solution, which was further sonicated for another 10 min. This process was repeated several times until the carbon nanomaterials were completely dispersed in the solution. The ultrasonication process causes decomposition of a radical initiator to initiate the polymerization process of vinylpyrrolidone, which leads to surface functionalization and good dispersion of carbon nanomaterials in the vinylpyrrolidone solution. During the polymerization process, oligomeric vinylpyrrolidone radicals, because of their high reactivity, will nonselectively attach to the unsaturated C=C double bonds of carbon nanomaterials, leading to homogeneous surface functionalization. The final solution was then diluted with ethyl alcohol, filtered through a Nylon 66 membrane (Supelco, 0.45 μm × 47 mm), and washed with ethyl alcohol several times to thoroughly remove physically absorbed polymers from the surface of carbon nanomaterials. The final products were then dried in a vacuum oven (at 70 °C) to remove the residual solvent. In the literature, free PVP polymer was commonly adopted as a dispersant polymer for stabilization of various kinds of metal nanoparticles, including Ag and Pb nanowires[27,28] noble metal nanoparticles,[29] and Te nanowires,[30] in organic solvents but was never chemically grafted onto carbon nanomaterials for application in DMFC. In this study, the process for surface-grafting PVPs onto carbon nanomaterials was developed, and the PVP-modified carbon nanomaterials were used as metal catalyst supports for DMFC for the first time.

Deposition of Pt, PtRu Nanoparticles on Carbon Nanosupports. Deposition of Pt and PtRu (1:1 atomic ratio) nanoparticles on carbon nanomaterials were achieved via two routes: all acid-oxidized carbon nanomaterials and Vulcan XC-72R carbon black form complexes with metal ions first, followed by reduction to metal nanoparticles (i.e., route I),[19,31] whereas all PVP-grafted carbon nanomaterials were chelated with premade metal nanoparticles directly (i.e., route II). The route I was schematically presented below. In route I, 250 mg of acid-oxidized carbon nanomaterial (MWCNT, GNF_H, or Vulcan XC-72R carbon black) was suspended in 50 mL of ethylene glycol solution, and then 8 mL of hexachloroplatinic acid (15 mg/mL) aqueous solution was added. The pH value of the solution was adjusted to 12.5 using a NaOH (12 M) stock solution and heated at 140 °C for 3 h. The Pt ions in the complex form (with the carboxylic acid groups of carbon nanomaterials)

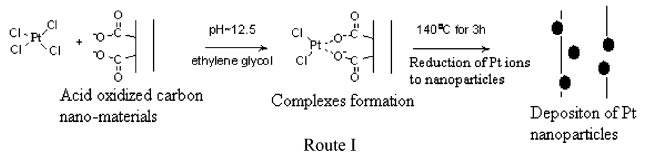

Route I

were chemically reduced to Pt nanoparticles by ethylene glycol. Finally, the Pt−AO-carbon nanocomposites (black solids) were filtered, washed with deionized water, and dried at 60 °C under a reduced pressure. Route II for preparation of surface-anchored Pt or PtRu nanoparticles is via direct complexation of premade metal nanoparticles with PVP-modified carbon nanomaterials. In route II, metal nanoparticles were prepared first before mixing with the PVP-modified carbon nanomaterials. To prepare Pt nanoparticles of 1−2 nm in diameters, 8 mL of hexachloroplatinic acid (H_2PtCl_6 with a concentration of 15 mg/mL) or $H_2PtCl_6-RuCl_3$ (in a 1:1 mole ratio, in the case of preparation of PtRu alloy) was dissolved in ethylene glycol. A 1 mL amount of NaOH

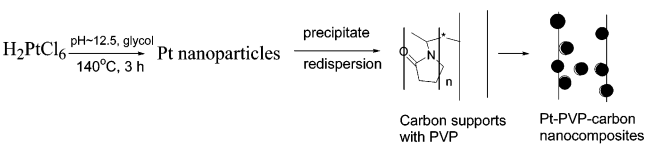

Route II

(12 M in water) was added to ethylene glycol to adjust the pH of the solution to about 12.5 and then heated at 140 °C for 3 h under a N_2 atmosphere. A transparent dark-brown homogeneous solution containing Pt or PtRu nanoparticles of 1−2 nm in diameter was obtained without

(22) Hwang, K. C. *J. Chem. Soc., Chem. Commun.* **1995**, 173.
(23) Tang, S. C.; Chen, Y. K.; Harris, P. J. F.; Green, M. L. H. *Nature* **1994**, *372*, 159.
(24) Singh, C.; Shaffer, M. S. P.; Windle, A. H. *Carbon* **2003**, *41*, 359.
(25) Ebbsen, T. W.; Ajayan, P. M. *Nature* **1992**, *358*, 220.
(26) Hsin, Y.-L.; Lai, J.-Y.; Hwang, K. C.; Lo, S.-C.; Chen, F.-R.; Kai, J. J. *Carbon* **2006**, *44*, 3328.
(27) Sun, Y. G.; Gates, B.; Mayers, B.; Xia, Y. N. *Nano Lett.* **2002**, *2*, 165.
(28) Wang, Y. L.; Herricks, T.; Xia, Y. N. *Nano Lett.* **2003**, *3*, 1163.
(29) Mu, X. D.; Evans, D. G.; Kuo, Y. A. *Catal. Lett.* **2004**, *97*, 151.
(30) Zhu, Y.; Wang, W.; Qi, R.; Hu, X. *Angew. Chem., Int. Ed.* **2004**, *43*, 1410.
(31) Antolini, E.; Cardellini, F. J. *Alloys Compd.* **2001**, *315*, 118.

forming precipitates.[31] The Pt or PtRu nanoparticles were precipitated using an aqueous HCl (1 M) solution to adjust the pH of the solution lower than 4. The precipitated Pt nanoparticles were collected by centrifugation and redispersed in ethanol to give a brown colored colloidal solution. To form Pt−PVP−carbon nanocomposites, 240 mg of the PVP-grafted carbon nanomaterial was dispersed in 20 mL of ethanol, and a Pt or PtRu nanoparticle-containing solution (containing ~50 mg of nanoparticles) was added drop by drop under vigorous stirring. Carbon nanomaterials form precipitates with Pt or PtRu nanoparticles very effectively via the surface-grafted PVP moieties immediately after addition of metal nanoparticles. The metal nanoparticle−carbon nanocomposites were collected by filtration, washed, and dried at 60 °C under vacuum overnight. The weight percentage of catalysts deposited on carbon supports was determined by inductively coupled plasma atomic emission spectrometry (ICP-AES, Jarrell-Ash model ICAP 9000). A sample of a known weight was soaked in aqua regia overnight, and the concentration of metal ions were characterized by ICP-AES. The weight percentage of metal catalysts deposited on carbon supports was calculated from the ICP-AES results.

Characterization of Pt−Carbon Nanocomposites. Various spectroscopic methods were used to characterize the surface-modified carbon nanocomposites, including FTIR (Bomen model DA83 FTS), X-ray photoelectron spectroscopy (ULVAC-PHI model Quantera SXM), and Raman (Triax 550 Jobin Yvon spectrometer using 632.8 nm from a He/Ne laser as the light source) spectroscopy. The weight percentage of surface-grafted PVP on carbon nanomaterials was determined using a thermal gravity analyzer at a rising temperature rate of 10 °C /min from 80 to 650 °C under a continuous argon gas flow with a flow rate of 100 sccm. The high-resolution transmission electron microscopic images (HRTEM) of metal nanoparticles were obtained from an analytic transmission electron microscopic meter (AEM, model JEM 2010, 200 kV) operated at 200 kV acceleration voltage. The X-ray diffraction (XRD) analysis was performed on a bed (Model D1) diffractometer over a 2θ range of 23−80° using Cu Kα radiation as the light source. The average crystalline size of Pt or PtRu nanoparticles deposited on carbon nanosupports was also obtained by fitting the diffraction peak Pt (220) using the Debye−Scherrer equation.[32] Electrochemical measurements were carried out using cyclic voltammetry (CV, CH instruments Model 600B).

Electrochemical Measurements of Pt−Carbon Nanocomposites. Electrochemical activities of various Pt−carbon nanocomposites were measured at room temperature in a conventional airtight three-electrode cell containing 1 M CH_4OH and 0.5 M H_2SO_4. A 20 mg amount of Pt−carbon nanocomposite was added to 1 mL of 2-propanal, which was then shaken for 30 min in an ultrasonic bath to form slurry. A volume of this slurry was brushed onto a piece of carbon paper (1.7 × 1.8 cm; ElectronChem EC-TP1-060) and dried in an oven at 80 °C for 20 min to remove the solvent. The weight of the carbon paper with dry carbon nanomaterials was measured and subtracted from that before coating of the slurry to obtain the loading of metal−carbon nanocomposites. Experiments were controlled so that ~3 mg of dried metal catalysts was deposited onto the carbon paper, which was later used as a working electrode for electrochemical measurements. A 100 μL amount of 5 wt % Nafion solution (Aldrich) was spread on top of the carbon nanocomposite layer and dried at 80 °C. Nafion acts as a protective layer to prevent loss of catalyst powder into the electrolyte solution. A platinum flat electrode with large area was used as the counter electrode, and an Ag/AgCl reference electrode was placed in the cell and connected to the working electrode. Cyclic potential was swept between 0.0 and 1.2 (vs NHE) at a rate of 20 mV·s^{-1}. The electrolyte was purged with N_2 gas for 30 min before the current measurements. In all experiments, stable voltammogram curves were recorded after 16 cycles of scanning. The electrochemically active surface (EAS) area of all samples was measured in a N_2 saturated H_2SO_4 (0.5 M) aqueous solution at a scan rate of 50 mV·s^{-1}. The chronoamperometry (current vs time response) was conduced in a H_2SO_4 (0.5 M)−CH_3OH (1 M) solution at a bias applied voltage of +0.6 V (vs Ag/AgCl reference electrode) for a period of 3000 s.

Scheme 2. A Schematic Chart of the Setup for Measurements of Electrical Conductivities of Carbon Nanomaterials

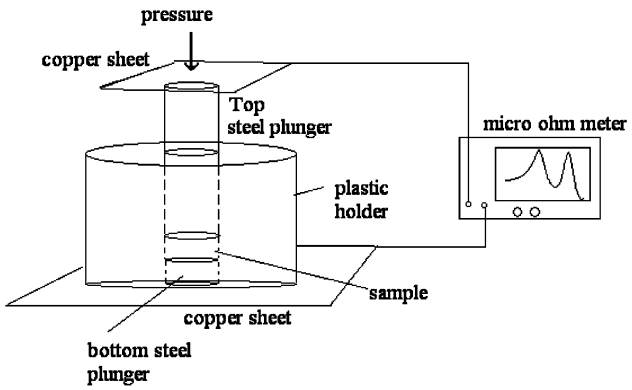

Measurements of Electrical Conductivities of Carbon Nanomaterials. The electrical conductivity (σ) of a pellet of a carbon nanomaterial was measured, by following a literature process,[33] at room temperature using a micro-ohmmeter (Delta United Instrument Corp, DU-5011). A 0.3 g amount of a carbon nanomaterial (without loading of metal catalysts) was dried at 80 °C overnight and compressed into a pellet in a hollow plastic cylinder with an inner diameter of 13 mm between two steel plungers at an externally applied pressure. The electric conductivity of the carbon nanomaterial was measured under a compression pressure of ~7 MPa. A schematic presentation of the setup for measurement of electrical conductivities is shown in Scheme 2. The sample height (L) was measured with a dial capliper from Mitutoyo Corporation. The electrical conductivity (σ, in a unit of S cm^{-1}) was given by eq 1

$$\sigma = \frac{L}{R*A} \tag{1}$$

where R is the resistance (Ω) and A is the area of the plunger surface.[33] By substituting the experimental values of L, A, and R, the electrical conductivity of a carbon nanomaterial can be obtained.

Results and Discussions

Spectroscopic Characterization of Pt−Carbon Nanocomposites. Surface-modified carbon nanomaterials were characterized by FTIR, TEM, and TGA. The FTIR spectra of AO-$MWCNT_{CVD}$ and PVP−$MWCNT_{CVD}$ were shown in Figure 1, and the FTIR spectra for AO- $MWCNT_{arc}$, PVP−$MWCNT_{arc}$, AO-GNF_H, and PVP−GNF_H were shown in Supporting Information, Figure S1. The AO-$MWCNT_{CVD}$ show the presence of very broad stretching band for hydroxyl groups at 3450 cm^{-1}, and $\nu_{C=O}$ stretching of carboxyl groups at ~1690 cm^{-1}. The characteristic $\nu_{C=O}$ and ν_{O-H} stretching bands from the surface-bound carboxylic acid groups were also observed in the other two acid-oxidized carbon nanomaterials, i.e., AO-GNF_H and AO-$MWCNT_{arc}$ (see Supporting Information, Figure S1). The PVP-grafted $MWCNT_{CVD}$ exhibit a strong characteristic lactam $\nu_{C=O}$ stretching band at 1662 cm^{-1} and a ν_{C-H} stretching absorption band at 2840−2980 cm^{-1}, which only appear in PVP-modified carbon nanomaterials (see Figures 1 and S1). For PVP-modified carbon nanomaterials, the strong and broad band at

(32) Wang, Y.; Ren, J. W.; Deng, K.; Gui, L. L.; Tang, Y. Q. *Chem. Mater*. **2000**, *12*, 1622.

(33) Pantea, D.; Darmstadt, H.; Kaliaguine, S.; Sümmchen, L.; Roy, C. *Carbon* **2001**, *39*, 1147.

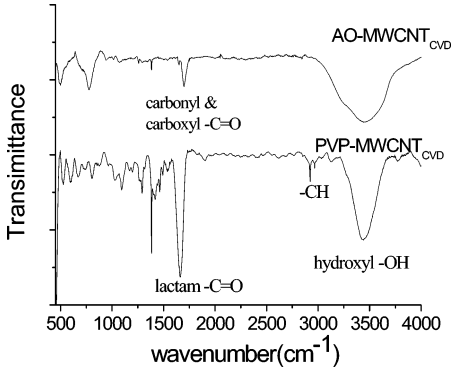

Figure 1. Fourier transformed IR spectra of acid-oxidized $MWCNT_{CVD}$ (top) and PVP-grafted $MWCNT_{CVD}$ (bottom).

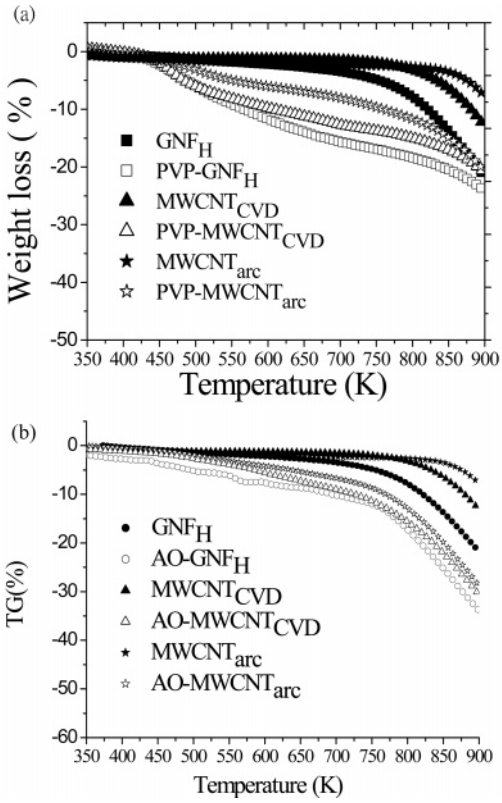

Figure 2. (a). The thermal gravimetric analysis of PVP-grafted as well as corresponding as-prepared carbon nanomaterials. (b) The thermal gravity analysis of acid-oxidized carbon nanomaterials.

3421 cm^{-1} is attributed to the O−H stretching (ν_{O-H}) of surface absorbed H_2O (by the PVP moieties). The weight percentage of surface-bound PVP moieties were determined using thermal gravimetric analysis (TGA). In Figure 2(a), the weight loss in the temperature range of 450−750 K is due to decomposition of surface-grafted PVP oligomers. For those carbon nanomaterials without surface-bound PVP, there is almost no weight loss in the temperature range of 450−750 K, and the onset of weight loss occurs at higher temperature region of 800−900 K, which is due to thermal decomposition of carbon nanomaterials themselves. The TGA results confirm that PVP oligomers were successfully grafted onto these carbon nanomaterials. From the difference in the weight loss between the as-prepared carbon nanomaterials and the corresponding PVP-grafted nanomaterials at 750 K, the amount of surface-bound PVP oligomers was estimated to be ∼12% for PVP−GNF_H, ∼12% for PVP−$MWCNT_{CVD}$, and ∼8% for PVP−$MWCNT_{arc}$, respectively. Similarly, from Figure 2(b), the weight percentages of surface-bound functional groups in acid oxidation-treated carbon nanomaterials were estimated to be ∼7% for AO-GNF_H, ∼10% for AO-$MWCNT_{CVD}$, and ∼6% for AO-$MWCNT_{arc}$, respectively. The relative extent of surface functionalization of carbon nanomaterials is determined by the total surface area and the chemical reactivity of carbon nanomaterials. The surface area of these carbon nanomaterials were also measured using the Brunauer−Emmet−Teller (BET) method at a bath temperature of 77 K using nitrogen gas as the adsorbate. The measured BET surface area (158.4 m^2/g) of GNF_H is larger than those of $MWCNT_{CVD}$ (77.8 m^2/g) and $MWCNT_{arc}$ (41.5 m^2/g). Since the oligomeric vinylpyrrolidone radicals are of very high chemical reactivity and their chemical reactions become nonselective, the carbon nanomaterials with higher surface area will have more PVP attached on their surface, which, in turn, will favor more metal nanoparticles being anchored on the surface.

Figure 3 shows the bright field TEM images of three representative nanocomposites, namely, Pt−PVP−GNF_H, Pt−AO-GNF_H, and Pt−PVP−$MWCNT_{CVD}$. The TEM images of other Pt−carbon nanocomposites, including Pt−AO-$MWCNT_{CVD}$, Pt−PVP−$MWCNT_{arc}$, Pt−AO-$MWCNT_{arc}$, and Pt−XC-72R, are shown in Figure S2 in Supporting Information. Figure 3(a) shows that the PVP-grafted GNF_H retain their characteristic herringbone graphene wall structures. From the TEM images, it can also be seen that small sized (∼1.8 nm in diameter, see also XPS results below) Pt nanoparticles distribute very evenly on the carbon nanomaterial. In contrast to the PVP-modified GNF_H, acid oxidation-treated GNF_H gave very hazy images (see Figure 3(b)), indicating severe structural damage caused by acid oxidation. Such acid oxidation-induced structural damage can also be observed in other carbon nanomaterials (see the contrast in Figure 3(c) vs Figure S2(a) for $MWCNT_{CVD,}$ and Figure S2-(b) vs Figure S2(c) for $MWCNT_{arc}$). The contrast in Figure S2-(c) is not as poor as those for the other carbon nanomaterials, which is attributed to the well graphitized wall structure and thus high chemical tolerance of $MWCNT_{arc}$. Another feature appearing in Figure 3(a) vs Figure 3(b) is that the distribution of Pt nanoparticles in PVP-modified GNF_H is very even, whereas for the acid-oxidized GNF_H, the distribution of Pt nanoparticles is very inhomogeneous, accompanied with formation of nanoparticle aggregates. Such a feature was also observed in other carbon nanomaterials (see the contrast in Figure 3(c) vs Figure S2(a) for $MWCNT_{CVD,}$ and Figure S2(b) vs Figure S2(c) for $MWCNT_{arc}$). From the TEM images, one can conclude that acid oxidation causes severe structural damage to most of carbon nanomaterials, where the PVP process creates much less structural damage than the acid oxidation method. The structural damage caused by the harsh acid oxidation condition not only affects the distribution of Pt nanoparticles, but will also cause a larger extent of loss in the electrical conductivity of carbon nanocomposites and thus worse electrocatalytic performance in the DMFC measurements than the corresponding PVP-grafted carbon nanomaterials (vide infra). Another important feature commonly seen in all PVP-grafted carbon nanomaterials is that very small Pt nanoparticles of 1.8 nm (see XRD measurements below) can be homogeneously distributed onto various carbon nanosupports (see Figures 3(a), 3(c), and Figures S2(b) and S2-(d)), which was not seen in acid oxidation-treated carbon nanomaterials.

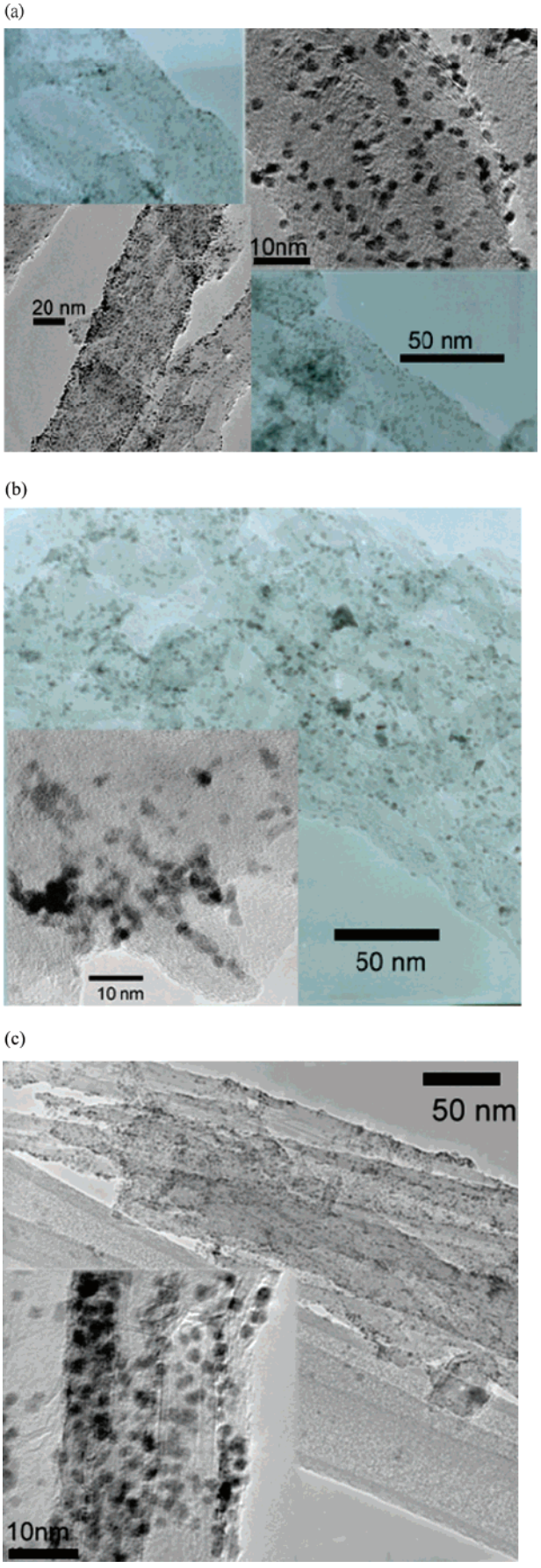

Figure 3. TEM images of (a) the Pt−PVP−GNF_H nanocomposite, (b) the Pt−AO-GNF_H nanocomposite, and (c) the Pt−PVP−$MWCNT_{CVD}$ nanocomposite.

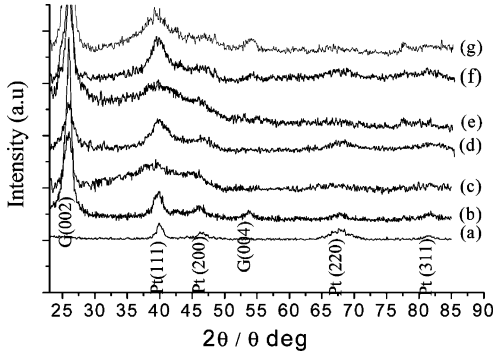

Figure 4. XRD patterns of various Pt−carbon nanocomposites: (a) Pt−XC-72 R, (b) Pt−AO-$MWCNT_{CVD}$, (c) Pt−PVP−$MWCNT_{CVD}$, (d) Pt−AO-GNF_H, (e) Pt−PVP−GNF_H, (f) Pt−AO-$MWCNT_{arc}$, (g) Pt−PVP−$MWCNT_{arc}$.

The XRD patterns of various Pt−carbon nanocomposites are shown in Figure 4. The diffraction peaks at 25.9° and 53.6° were assigned to the graphite crystallographic planes (002) and (004) of MWCNT, respectively. The characteristic diffraction peaks Pt(111) at 39.6°, Pt(200) at 46.3°, Pt(220) at 67.4° , and Pt(311) at 81.4° for a face-centered cubic (fcc) structure were also observed. In Figure 4, there exist two noticeable features: (1) the Pt (111) band at ∼40° is very broad for all PVP-modified carbon nanomaterials (i.e., samples **c**, **e**, and **g**), which is in contrast to those sharp and narrow bands for all acid oxidation-treated carbon nanomaterials (i.e., samples **b**, **d**, and **f**) and carbon black (sample a). Previously, it was reported that the electrocatalytic activity of Pt nanoparticles toward methanol oxidation is maximized for the Pt(111) crystallographic surface.[34] (2) Another noticeable feature is that the Pt(220) band at ∼68° is very broad and weak for these PVP-modified carbon nanocomposites (i.e., samples **c**, **e**, and **g**) but is clearly seen for the rest of acid oxidation-treated samples. These features are readily explained by Scherrer's equation[31] (see eq 2).

$$L = \frac{0.9\lambda}{B_{(2\theta)} \cos \theta_{\max}} \qquad (2)$$

where L is the mean size of the Pt nanoparticles, λ is the wavelength of the X-ray source [i.e., λ(Cu, Kα)= 1.5418 Å], $\theta_{\max}$ is the angle at peak maximum (in radians) of a chosen XRD peak, and $B_{(2\theta)}$ is the full-width at half-maximum of the chosen XRD peak. According to Scherrer's equation, the larger the mean size (L) of Pt nanoparticles, the smaller the full-width at half-maximum ($B_{2\theta}$). The mean size (L) is inversely proportional to the $B_{2\theta}$. The differences in the band intensities and shapes of the Pt(111) diffraction peak at 39.6° for different nanocompsites are due to the differences in the sizes of the deposited Pt nanoparticles. To obtain the mean sizes of deposited Pt nanoparticles for different nanocomposites, the Pt(220) band at ∼68° was fitted by the Scherrer's equation (see Figure 5). The Pt(220) band, instead of the Pt(111) band, was chosen for fitting, because this band does not have interference from other peaks and therefore can provide better accuracy. The average sizes of Pt nanoparticles so obtained are as follows: AO-$MWCNT_{arc}$ (3.1 nm), AO-$MWCNT_{CVD}$ (2.9 nm), XC-72R (2.8 nm), and AO-GNF_H (2.6 nm). The average size of free Pt nanoparticles prepared by refluxing Pt precursors (i.e., hexachlo-

(34) Chrzanowski, W.; Kim, H.; Wieckowski, A. *Catal. Lett.* **1998**, *50*, 69.

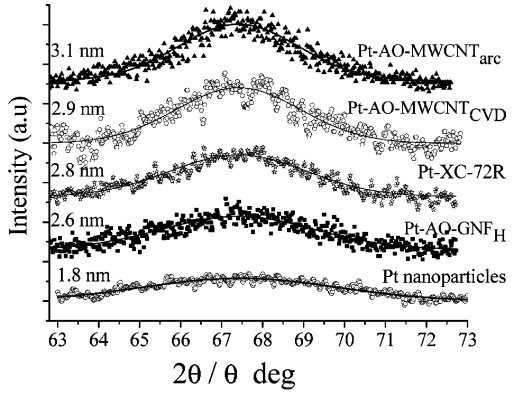

Figure 5. The Pt(220) XRD bands of various carbon nanomaterials were fitted by Scherrer's equation (see the text) to obtain the average sizes of Pt nanoparticles. For the purpose of comparison, the XRD band of free Pt nanoparticles (without deposition on carbon nanomaterials) was also inserted as the bottom trace in the figure.

roplatinic acid) in ethylene glycol[15] is ~1.8 nm (the lowest curve in Figure 5). The mean size of Pt nanoparticles in all PVP-modified carbon nanocompsites is the same as that of free Pt nanoparticles, i.e., ~ 1.8 nm, since the deposited Pt nanoparticles are premade before anchoring onto PVP-modified carbon nanomaterials. Because of the smaller sizes of the deposited Pt nanoparticles, the Pt(111) bands in all PVP-modified nanocomposites are broadened, leading to the observed discrepancies in band shapes between PVP and AO-treated nanocomposites in Figure 4. According to Scherrer's equation, for a given mean size (L) of Pt nanoparticles, the particle-size-dependent line broadening ($B_{(2\theta)}$) is inversely proportional to the diffraction angle (cos θ_{max}). Therefore, the line broadening phenomenon becomes much more serious for the Pt(220) band at ~68° than for the Pt(111) at 39.6°, leading to the very broad (and thus weak) Pt(220) bands for all PVP-modified nanocomposites in Figure 4.

The average size of Pt nanoparticles deposited on the acid-oxidized carbon nanomaterials via the impregnation−reduction process is significantly affected by the amount of the surface functional groups, which, in turn, are proportional to the surface area of carbon nanomaterials. In terms of the surface area, the Vulcan XC-72R carbon black (250 $m^2\ g^{-1}$) is larger than the other three carbon nanomaterials, GNF_H (158.4 $m^2\ g^{-1}$), $MWCNT_{CVD}$ (77.8 $m^2\ g^{-1}$), and $MWCNT_{arc}$ (41.5 $m^2\ g^{-1}$). The XC-72R carbon black was used as received without being further treated by acid oxidation, and therefore it is difficult to compare the amount of surface functional groups with the other three nanomaterials. Whereas for GNF_H, $MWCNT_{CVD}$, and $MWCNT_{arc}$, they were treated by the same acid oxidation process. Therefore, the sizes of Pt nanoparticles (AO-$MWCNT_{arc}$, 3.1 nm > AO-$MWCNT_{CVD}$, 2.9 nm > AO-GNF_H, 2.6 nm) are inversely proportional to the surface area (AO-$MWCNT_{arc}$ < AO-$MWCNT_{CVD}$ < AO-GNF_H). In general, the larger the surface area, the smaller the Pt nanoparticle deposited. For the same amount of loading of Pt nanoparticle catalyst, the smaller the metal nanoparticle size, the higher the electrochemically active surface (EAS) area. For these PVP-grafted carbon nanomaterials, the Pt nanoparticles are from premade nanoparticles and have the same value of ~1.8 nm.

The Raman spectra of acid-oxidized, PVP-grafted, and the as-prepared carbon nanomaterials are shown in Figure 6. The peak at 1350 cm^{-1} is assigned to the A_{1g} breathing mode of

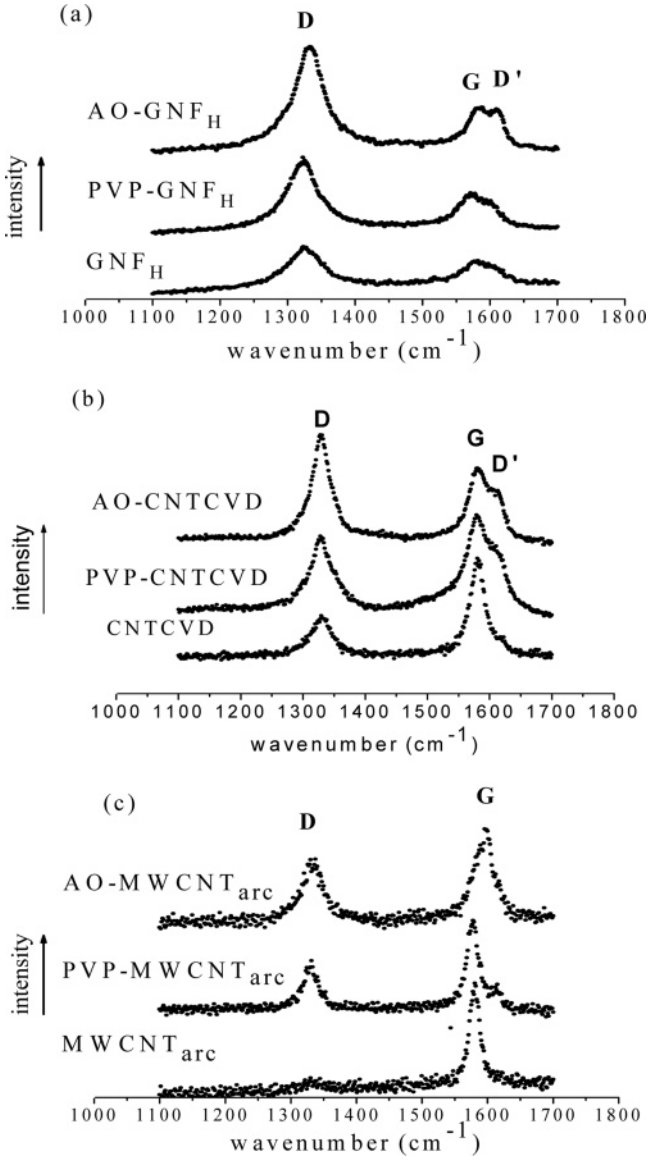

Figure 6. Raman spectra of various carbon nanomaterials: (a) AO-GNF_H, PVP−GNF_H, and pristine GNF_H; (b) AO-$MWCNT_{CVD}$ and PVP−$MWCNT_{CVD}$, pristine $MWCNT_{CVD}$; (c) AO-$MWCNT_{Arc}$, PVP−$MWCNT_{Arc}$, and pristine $MWCNT_{Arc}$.

disordered graphite structure (i.e., the D band), and the high-frequency peak at ~1580 cm^{-1} assigned to the E_{2g} stretching mode of graphite (i.e., the G band). The G band reflects the structure of the sp^2 hybridized carbon atom.[35,36] An additional side band at ~1620 cm^{-1} was also observed, which is assigned as the D′ band. Both the D and the D′ bands are due to defect sites in the hexagonal framework of graphite materials. The height of the D peak usually increases upon surface modification of carbon nanomaterials.[26] The extent of the defects in graphite materials upon surface modification can be quantified by the intensity ratio of the D to G bands (i.e., I_D/I_G). The intensity ratios of I_D/I_G for various carbon nanomaterials with and without surface modification are listed in Table 1. The I_D/I_G ratios are 1.51, 1.74, and 1.81 for the as-prepared GNF_H, PVP− GNF_H, and AO-GNF_H, respectively, 0.61, 0.76, and 1.41 for the as-

(35) Park, K. W.; Kwon, B. K.; Choi, J. H.; Park, I. S; Kim, Y. M.; Sung, Y. E. *J. Power Sources.* **2002**, *109*, 439.
(36) Ferrari, A. C.; Robertson, J. *Phys. Rev. B* **2000**, *61*, 14095.

Table 1. Characteristic Values for Pt−Carbon Nanocomposites **a**−**g**

carbon support	XC-72R Carbon black (**a**)	AO-MWCNT$_{CVD}$ (**b**)	PVP–MWCNT$_{CVD}$ (**c**)	AO-GNF$_H$ (**d**)	PVP–GNF$_H$ (**e**)	AO-MWCNT$_{arc}$ (**f**)	PVP–MWCNT$_{arc}$ (**g**)
Pt (wt %)[a]	14.1	13.8	15.0	15.4	14.5	15.2	14.2
Pt size[b] (nm)	2.8	2.9	1.8	2.6	1.8	3.1	1.8
BET ($m^2\,g^{-1}$)	250	77.8	77.8	158.8	158.8	41.5	41.5
EAS $m^2\,g^{-1}$ Pt	87	79	95	85	117	76	91
conductivity (S cm^{-1})	7.6	6.5	7.4	1.4	7.3	14.2	17.4
Raman D/G ratio	very broad	1.41	0.76	3.18	1.54	0.71	0.61
E_{max} (V)[c]	0.91	1.00	1.02	0.907	1.02	1.02	1.05
$I_{0.8V}$[d] mA $cm^{-2}\,mg^{-1}$ Pt	35.2	38.7	45.3	23.5	104.6	57.9	73.1
I_{max}[e] mA $cm^{-2}\,mg^{-1}$ Pt	62.2	85.5	106.7	41.5	234	134.1	172.7

[a] Metal composition was determined by ICP-AES. [b] Values determined from XRD data. [c] E_{max}: peak potential. [d] $I_{0.8V}$: current density at $E = 0.8$V. [e] I_{max}: peak current density.

prepared MWCNT$_{CVD}$, PVP−MWCNT$_{CVD}$, and AO-MWCNT$_{CVD}$, and 0.12, 0.61, and 0.71 for the as-prepared MWCNT$_{arc}$, PVP−MWCNT$_{arc}$, and AO-MWCNT$_{arc}$. A clear trend can be seen that the I_D/I_G ratio increases for all carbon nanomaterials upon surface modification, and the acid-oxidized carbon nanomaterials have a higher I_D/I_G ratio (or more structural damage) than that for the corresponding PVP-grafted carbon nanomaterials. This trend is consistent with the TEM results shown in Figure 3, where more structural damage is accompanied by a worse contrast and blurred images in all acid-oxidized samples than those for the corresponding PVP-treated nanomaterials. Such structural damage or defects on the graphene layers are accompanied with decreases in the electrical conductivity of the carbon nanosupports (see conductivity results below). Both the Raman and the TEM measurements (as well as electrical conductivity measurements, vide infra) lead to the same conclusion that the PVP surface modification process is less destructive to the graphene layers than the acid oxidation process. The electric conductivity of the carbon nanosupports could be a decisive factor determining the maximum current density and overall performance of DMFC.

Figure 7(a) shows the XPS spectra of carbon nanocomposites a−g. Besides the C(1s) signal at 284.2 eV, O(1s) at 543.1 eV, and O (KLL) at 986 eV, the Pt(4f), Pt($4d^5$), and Pt($4d^3$) signals appear in all samples. Notice that the Pt signals from PVP-grafted samples are stronger than those of corresponding acid-oxidized samples. Since XPS is sensitive to the surface composition of samples,[37] the much higher Pt signal intensities in PVP-grafted samples indicate that PVP-treated carbon nanomaterials can load a larger amount of Pt nanoparticles per unit area than those of acid oxidation-treated samples. The N(1s) signal at 409.9 eV originates from the pyrrolidone groups of the surface-grafted PVP moieties on the carbon nanomaterials and was observed only in the PVP-modified samples but not in acid-oxidized samples. The Pt(4f) signals at 71.4 and 74.9 eV in Figure 7(b) reveal that the deposited Pt nanoparticles are in a metallic form, instead of ionic forms.

Electrical Conductivities of Carbon Nanomaterials. Unlike carbon supports in other applications, the anodic carbon supports in DMFC not only provide large surface area for dispersion of metal catalyst nanoparticles but also have to transport the oxidation electrons to the cathode to complete a cell cycle. Therefore, the DMFC performance of a nanocomposite depends strongly on its electrical conductivity, which was rarely measured and its effects on DMFC performance discussed. To

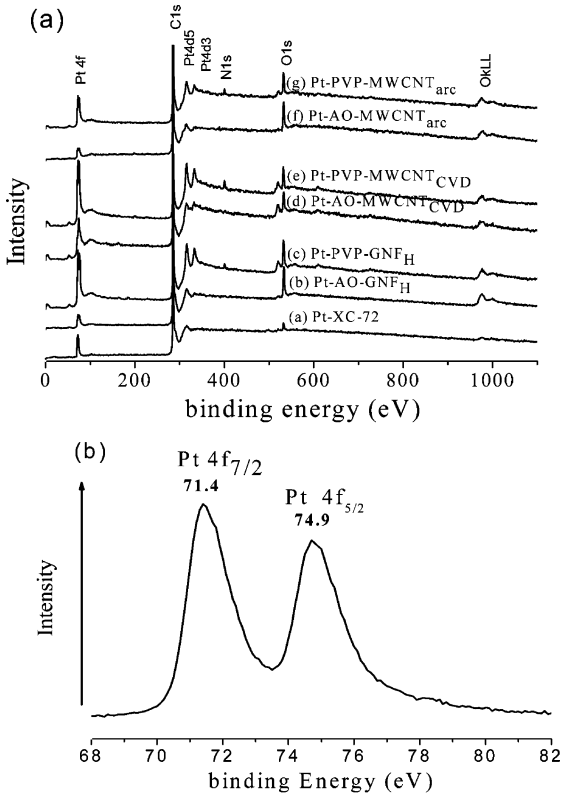

Figure 7. (a) XPS spectra of various Pt−carbon nanocomposites, and (b) XPS core level spectra of the Pt(4f) bands.

elucidate their effects on the DMFC performance, electrical conductivities of various carbon nanomaterial powders with or without surface functionalization were measured and shown in Figure 8. The electrical conductivities of carbon nanomaterial powders are strongly dependent on the distances and interfaces between nanoparticles. As the inter-nanoparticle distances become shorter at high compression pressures, the measured electrical conductivity will gradually approach the intrinsic value for each nanomaterial.[33] Previously, it was shown that above an applied pressure of 2 MPa, the electric conductivities of many carbon nanomaterials start approaching the final intrinsic value. In this study, the externally applied pressure of 7 MPa is higher than the reported threshold pressure of 2 MPa. Therefore, the values of electrical conductivities in Figure 8 can be regarded as a quasi-intrinsic electric conductivity of each carbon nanomaterial. The measured quasi intrinsic electrical conductivity of 7.6 S cm^{-1} is close to the value previously reported "extrapolated" value of 7.4 S cm^{-1} for Vulcan XC-72R carbon black.[33] Figure 8 shows that the electrical conductivity (∼31 S cm^{-1}) of as-prepared MWCNT$_{are}$ is highest, ∼2 fold of those

(37) Chastain, J. *Handbook of X-ray Photoelectron Spectroscopy*: Perkin-Elmer Corporation, Eden Prairie, 1992.

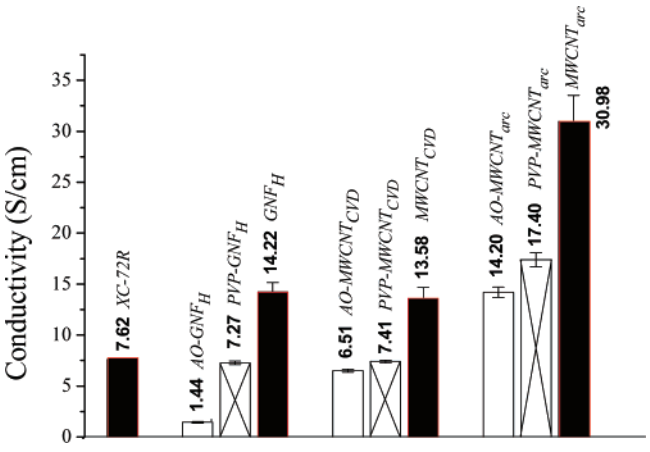

Figure 8. The electrical conductivity of carbon nanomaterials pellets at an externally applied pressure of 7 MPa at room temperature.

of graphite carbon nanofibers (~14.2 S cm^{-1}) and $MWCNT_{CVD}$ (~13.6 S cm^{-1}), and ~4 fold of that of the Vulcan XC-72R carbon black (~7.6 S cm^{-1}). Two noticeable features could be seen in Figure 8. The first one is that the electrical conductivities of all surface-modified carbon nanomaterials are smaller than those of corresponding as-prepared materials. The second feature is that the PVP-modified carbon nanomaterials have higher electrical conductivities than all the corresponding AO-modified nanomaterials. The loss in the electrical conductivity is mostly due to structural damage upon surface modification. Although surface functionalization has the disadvantage of loss in the electrical conductivities of carbon supports, it is still necessary to carry out surface modification of carbon supports since the advantages of increasing the EAS value (via introducing large amount of surface metal binding sites, prevention of metal catalyst aggregation) can still overcome the disadvantages if a proper surface modification process is adopted. The second feature is consistent with the TEM and the Raman measurements that PVP surface modification causes much less structural damage than does the acid oxidation process. The extent of loss in the electrical conductivity (or structural damage) is dependent on the nature of carbon nanomaterials as well as the amount of surface functional groups attached. Because of the characteristic structural features, graphite carbon nanofiber is much more vulnerable to acid oxidation-induced structural damage than CNT. Upon acid oxidation, GNF_H gains ~6 wt % of surface functional groups but loses 90% of its electrical conductivity. Its residual conductivity is only 8% of that of $AO\text{-}MWCNT_{arc}$, or ~ 19% of those of the $AO\text{-}MWCNT_{CVD}$ and Vulcan XC-72R carbon black. In sharp contrast, the $PVP-GNF_H$ retains 51% of the conductivity of GNF_H with ~12 wt % gain in weight from the surface-grafted PVP oligomers. The results in Figure 8 clearly show that the PVP grafting process is superior to the acid oxidation process. Not only does the PVP process attach more wt% of surface functional groups, but it also retains larger percentages of electrical conductivity.

From Figure 8, it can be seen that the electrical conductivity of $AO\text{-}MWCNT_{arc}$ is about 2 fold of those of $AO\text{-}MWCNT_{CVD}$ and Vulcan XC-72R carbon black. The electrical conductivities of $AO\text{-}MWCNT_{CVD}$ and Vulcan XC-72R carbon black are compatible to each other. Previously, the presumed "better" electrical conductivity of Pt−AO-MWCNT is believed to be responsible for the higher electrocatalytic performance toward methanol oxidation than Pt−Vulcan XC-72R carbon black,[16,17,19,21]

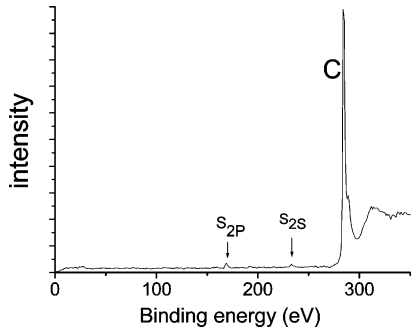

Figure 9. X-ray photoelectron spectroscopic spectrum of Vulcan XC-72R carbon black.

despite that the average surface area of MWCNT (20−60 m^2 g^{-1})[21] is only about one-fifth of that (~250 m^2 g^{-1}) of the Vulcan XC-72R carbon black. The electrical conductivity data shown in Figure 8 suggests that the electric conductivity cannot be the factor responsible for the literature-reported superior DMFC performance of MWCNT than Vulcan XC-72R carbon black. In terms of the combined effects of electrical conductivity and total surface area of carbon supports, Vulcan XC-72R carbon black is much better than MWCNT, contradicting the observed better DMFC performance for MWCNT-based nanocompsites. Then what are the factors causing poor DMFC performance in Vulcan XC-72R carbon black-based nanocomposites? One possible cause is the sulfur poisoning of the Pt catalysts. It was known that Vulcan XC-72R carbon black has 0.5 atomic percentage of sulfur atoms on the graphene layer surface.[33] Sulfur atoms are well-known to be very poisonous to Pt catalysts.[38] To confirm the possibility of "sulfur poisoning" in our Vulcan XC-72R carbon black sample, elemental analysis was carried out. The elemental analysis result indicates that Vulcan XC-72R carbon black did contain 0.43 atomic percent of sulfur element (data not shown), which is close to the value of 0.5% reported by others in the literature.[33] Sulfur poisoning of Pt or PtRu metal catalysis, however, could only occur on the surface of carbon supports. We therefore carried out XPS surface analysis of the Vulcan XC-72R carbon black (see Figure 9). The XPS measurement is sensitive to the surface composition at a depth of ~2.3 nm (for carbon based samples). The XPS measurement shows the presence of S(2p) and S(2s) signals at 168.5 and 233 eV, respectively. After removal of a nonlinear background from the spectra, using a mixed Gaussian−Lorentzian function to fit the bands, and correction of the cross-sections of carbon and sulfur elements, the atomic percentage of sulfur atom on the surface was found to be ~0.74%, slightly higher than the percentage of the bulk composition. Overall, both elemental analysis and XPS measurements confirm the presence of sulfur atoms and the likely poisoning of Pt(Ru) catalysts on the Vulcan XC-72R carbon black. In addition to the sulfur poisoning problem, Vulcan XC-72R carbon black has micropores on the surface. The mass transport to the metal catalysts located inside these micropores has been reported to be very poor.[39] Most probably, the retardation effects of sulfur-poisoning and micropores of Vulcan XC-72R carbon black are the key factors reversing the electrocatalytic performance of the carbon black over MWCNT.

The conductivity data in Figure 8 show that the arc-discharged MWCNT do have advantages in electrical conductivity over

(38) Rodriguez, J. A.; Hrbek, J. *Acc. Chem. Res.* **1999**, *32*, 719.
(39) Anderson, M. L.; Stroud, R. M.; Rolison, D. R. *Nano Lett.* **2002**, *2*, 235.

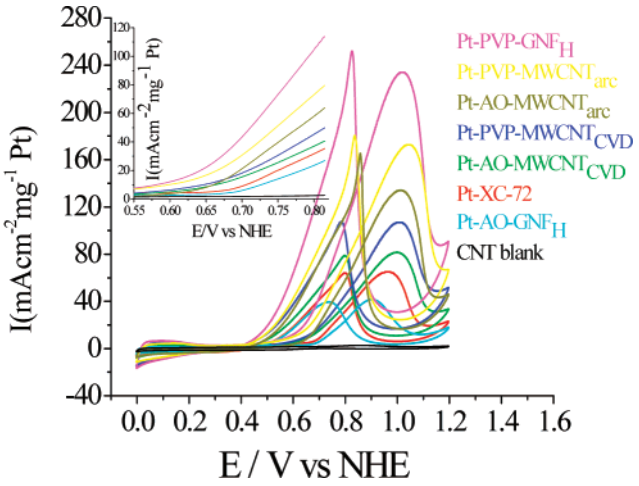

Figure 10. Cyclic voltametric curves of Pt−carbon nanocomposites in a H_2SO_4 (0.5 M)−CH_3OH (1 M) aqueous solution saturated with N_2 gas. The scanning rate of the applied voltage is 20 mV/s. The forward parts of the CV curves were shown as an inset in the figure. The currents were normalized to the loading (or weight) of Pt catalysts.

other carbon nanomaterials: ~31 S cm^{-1} for MWCNT$_{arc}$, 7.6 S cm^{-1} for Vulcan XC-72R carbon black, 14.2 S cm^{-1} for GNF$_H$, and 13.6 S cm^{-1} for MWCNT$_{CVD}$. However, the surface area (41.5 m^2/g) of MWCNT$_{arc}$ is only ~26% of graphite carbon nanofibers (158.4 m^2/g), or ~17% of Vulcan XC-72R carbon black (~250 m^2/g). For applications relying on the surface area but not on electrical conductivity, MWCNT$_{arc}$ will not be a good choice. MWCNT$_{CVD}$ has a larger surface area than those from arc-discharge processes, but the electrical conductivity is only about half that of MWCNT$_{arc}$. The MWCNT$_{arc}$ are more resistant toward the corrosive acid oxidation process. The electrical conductivity of AO-MWCNT$_{arc}$ is about two times that of AO-MWCNT$_{CVD}$. The straight and clear-edged graphite walls taken from the AO-MWCNT$_{arc}$ (see Figure S2 (c)) is in sharp contrast to the blurred images for the AO-MWCNT$_{CVD}$. The Raman I_D/I_G ratio for the AO-MWCNT$_{arc}$ is still lower than those of both PVP−MWCNT$_{CVD}$ and AO-MWCNT$_{CVD}$. Therefore, the better structural integrity and electrical conductivity of MWCNT$_{arc}$ nanocomposites (**g** and **f**) are the key factors leading to the higher electrocatalytic performance than the corresponding MWCNT$_{CVD}$ nanocomposites (**f** > **b**, and **g** > **c**).

Electrocatalytic Performance. To investigate the electrocatalytic activity of various Pt−carbon nanocomposites, cyclic voltametric measurements of the methanol oxidation reaction (MOR) were carried out in H_2SO_4 (0.5 M)−CH_3OH (1.0 M) aqueous solution at room temperature (see Figure 10). The solutions were bubbled with N_2 gas for 30 min to remove molecular oxygen right before the CV measurements. The Faradaic current exhibits the well-known dependence on the electrode for the MOR on carbon-supported Pt catalyst.[40,41] The forward anodic peak around 1.0 V_{NHE} is due to oxidation of methanol. The maximum peak current is designated as, I_{MeOH}. In the backward scan, the oxidation peak at ~0.8 V_{NHE} is attributed to the oxidation of adsorbed CO or CO-like species, which were generated via incomplete oxidation of methanol in the forward scan. This maximum peak current is designated as, I_{CO}. A large ratio of I_{MeOH}/I_{CO} represents a more complete methanol oxidation, less accumulation of CO-like species on the catalyst surface, and thus a better CO-tolerance.[7,42] The I_{MeOH}/I_{CO} ratios for all nanocomposites do not have a large difference, ranging from 0.93 to 1.02, indicating that all Pt catalysts still suffer a significant extent of CO-induced partial deactivation, irrelevant to which carbon support was used. The forward parts (0.55−0.85 V_{NHE}) of the methanol oxidation curves are displayed as an inset in the Figure 10. From the magnitude of electrocatalytic currents, it can be seen that the catalytic performance of the Pt−carbon nanocomposites decreases in the following order: Pt−PVP−GNF$_H$ (**e**) > Pt−PVP−MWCNT$_{arc}$ (**g**) > Pt−AO-MWCNT$_{arc}$ (**f**) > Pt−PVP−MWCNT$_{CVD}$ (c) >Pt−AO-MWCNT$_{CVD}$ (**b**) > Pt−XC-72R (**a**) > Pt−AO-GNF$_H$ (**d**). Nearly all of MWCNT and GNF$_H$ nanocomposites have higher electrocatalytic currents than the Pt−XC-72 R carbon black nanocomposite. In the CVs obtained in the 0.5 M H_2SO_4 solution (see Supporting Information Figure S6(a) and S6(b)), the cathodic and anodic peaks appearing between 0.0 and 0.3 V_{NHE} originate from the adsorption and desorption of molecular H_2 on the surface of Pt nanoparticles deposited on carbon supports. By using the double layer charging current of Pt as a baseline and the standard 0.22 mC per real cm^2 as a conversion factor, the area of H_2 adsorption and desorption on CV patterns can be used to determine the values of electrochemically active surface (EAS) area for Pt nanoparticles[40,43] deposited on carbon supports. Table 1 summarizes the XRD, Raman, catalytic performance, and EAS values of Pt−carbon nanocomposites **a**−**g**. The results in Table 1 show a noticeable feature that all PVP-modified carbon nanocomposites exhibit higher electrocatalytic activities than the corresponding carbon nanocomposites treated by acid oxidation (i.e., **c** > **b**, **d** > **e**, and **g** > **f**). The reasons for the above observation could be that the PVP-grafted carbon nanomaterials have the following superior features over the acid-oxidized samples: smaller sizes of Pt nanoparticles, better dispersion, larger total Pt surface area, and better electric conductivity (see results in Figure 8). These superior features were supported by the observation of larger EAS values for the PVP-grafted nanocomposites (see Table 1). Furthermore, the I_D/I_G Raman intensity ratios and TEM results (as discussed before) all consistently point to the same conclusion that the PVP process causes much less structural damage on carbon nanomaterials, better electrical conductivity, and thus better DMFC performance than the acid oxidation process. The integrity of the graphene structures (and thus the electric conductivity) of carbon supports is a very crucial factor determining the electrocatalytic performance of Pt−carbon nanocomposites.

Among all Pt−carbon nanocomposites, the Pt−PVP−GNF$_H$ nanocomposite **e** has the best performance. In the sharp contrast, the Pt−AO-GNF$_H$ nanocomposite **b** gives the worst performance among all. The data in Figure 8 show that the electrical conductivity of AO-GNF$_H$ is only 1.4 S cm^{-1}, which is about one-fifth of the conductivity for PVP−GNF$_H$. This result highlights the importance of electrical conductivity of carbon supports to the overall DMFC performance of an anodic nanocomposite, as well as the importance of the choice of

(40) Pozio, A.; De Francesco, M.; Cemmi, A.; Cardellini, F.; Giorgi, L. *J. Power Sources* **2002**, *105*, 13.
(41) Herrero, E.; Franasazczuk, K.; Wieckowski, A. *J. Phys. Chem.* **1994**, *98*, 5074.
(42) Deivaraj, T. C.; Lee, J. Y. *J. Power Sources* **2005**, *142*, 43.
(43) Perez, J.; Gonzalez, E. R.; Ticianelli, E. A. *Electrochim. Acta* **1998**, *44*, 1329.

surface functionalization processes Previously, E. S. Steigerwalt et al.[4] reported that their surface-unmodified PtRu−GNF_H nanocomposite, showing the best DMFC performance, has the lowest resistance among all carbon nanomaterials investigated in their studies, supporting the importance of the electrical conductivity of carbon supports for the overall DMFC performance. The very poor electrical conductivity of AO-GNF_H is certainly the key factor responsible for its very poor DMFC performance. The very low electrical conductivity of AO-GNF_H is consistent with the TEM and Raman observations that the AO-GNF_H has serious structural damage. The very poor electric conductivity of AO-GNF_H cancels out the positive contribution from the favorable factor of the large total surface area. Therefore, the poor electrical conductivity of the AO-GNF_H (vide supra) could be the key factor reversing the electrocatalytic performance from the best Pt−PVP−GNF_H to the worst Pt−AO-GNF_H. The best performance of the Pt−PVP−GNF_H nanocomposite **e** could be a result of the combined effects of large surface area and reasonably good electrical conductivity, and the large EAS value of the deposited Pt nanoparticles. Although, the size (1.8 nm) of Pt nanoparticles deposited on these carbon nanosupports (i.e., PVP−GNF_H, PVP−$MWCNT_{CVD}$, and PVP−$MWCNT_{arc}$) are the same (all via chelation of the same premade Pt nanoparticles), the BET surface area of GNF_H (158.4 m^2/g) is 2 to 4 fold larger than those of $MWCNT_{CVD}$ (77.8 m^2/g) and $MWCNT_{arc}$ (41.5 m^2/g), resulting in larger loading capacity of Pt nanoparticles in the nanocomposite **e**, or much less aggregation (or larger EAS) at the same weight percent loading of Pt nanoparticles. In this study, the weight percent loadings of Pt nanoparticles were controlled to be about the same, but the measured EAS value (normalized by the weight of Pt, see Table 1) of the nanocomposite **e** is larger than those for the nanocomposites **d** and **g**. The difference in the EAS values among PVP-grafted nanomaterials (**e**, **d**, and **g**) is probably due to the difference in the surface area of carbon nanomaterials (and thus the extent of aggregation of Pt nanoparticles).

From the above results, it seems clear that for a chosen metal catalyst, the electrocatalytic performance of a DMFC is mostly determined by the following three key factors: (1) surface area (SA) of carbon supports, (2) the EAS value of metal nanoparticles, and (3) electrical conductivity (EC) of carbon supports. A large surface area of carbon supports can lead to more surface functional groups, a larger amount of metal catalyst nanoparticles being loaded, and less aggregation of metal nanoparticles. The values of the above three factors for various carbon nanomaterials are listed in Table 1. The normalized values of SA*EAS*EC for various carbon nanomaterials are in a deceasing sequence: Pt−PVP−GNF_H (**e**: 3.40) > Pt−PVP−$MWCNT_{arc}$ (**g**: 1.65) > Pt−PVP−$MWCNT_{CVD}$ (**c**: 1.37) > Pt−AO-$MWCNT_{arc}$ (**f**: 1.12) > Pt−AO-$MWCNT_{CVD}$ (**b**: 1.0) > Pt−AO-GNF_H (**d**: 0.47). The Vulcan XC-72R carbon black was excluded from the comparison, since it has two additional lethal and unfavorable factors, namely, the "sulfur-poisoning" and the "poor mass transport in micropores" problems[39] which were discussed previously in Electrical Conductivities of Carbon Nanomaterials. The ranking of the SA*EAS* EC values qualitatively matches the observed I_{max} (see Table 1): Pt−PVP−GNF_H (**e**: 234 mA cm^{-2} mg^{-1} Pt) > Pt−PVP−$MWCNT_{arc}$ (**g**: 172.7) > Pt−AO-$MWCNT_{arc}$ (**f**: 134.1) > Pt−PVP−$MWCNT_{CVD}$ (**c**: 106.7) > Pt−AO-$MWCNT_{CVD}$ (**b**: 85.5) > Pt−AO-GNF_H (**d**: 41.5). The only mismatch is the reverse sequence of Pt−AO-$MWCNT_{arc}$ (**f**) and Pt−PVP−$MWCNT_{CVD}$ (**c**). The Pt−AO-$MWCNT_{arc}$ (**f**) has smaller surface area and EAS values, but higher electrical conductivity (as well as better DMFC performance) than that of Pt−PVP−$MWCNT_{CVD}$ (**c**), indicating that the electrical conductivity seems to have a more important contribution to the overall DMFC performance than the other two factors.

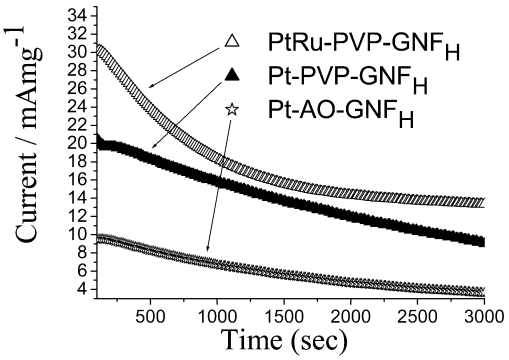

Figure 11. Chronoamperometry curves for PtRu(1:1)-PVP−GNF_H, Pt−PVP−GNF_H and Pt−AO-GNF_H in H_2SO_4 (0.5 M) + CH_3OH (1.0 M) at an applied voltage of 0.6 V. The electrocatalytic currents were normalized to the weight of the metal catalyst. In the case of PtRu, the weight of PtRu alloy was used, instead of the weight of Pt alone.

Comparison of Electrocatalytic Performance of PtRu− and Pt−Carbon Nanocomposites. To show that surface chelation of metal nanoparticles onto PVP-grafted carbon nanomaterials is a general process, PtRu alloy nanoparticles were prepared in advance, followed by mixing with PVP-grafted carbon nanomaterials. Their electrocatalytic performance for methanol oxidation reactions was then examined. The procedure for preparation of PtRu nanoparticles is the same as that for Pt nanoparticles, except that a 1:1 mole ratio of H_2PtCl_2 and $RuCl_3$ was used to replace the hexachloroplatinic acid in the preparation of metal nanoparticles. The PtRu alloy nanoparticles were precipitated, collected by centrifugation, and redispersed in an ethyl alcohol solution containing PVP−GNF_H nanomaterials. Upon mixing, the PtRu nanoparticles and GNF_H form precipitates, which were then filtered, washed with ethyl alcohol several times, and dried in vacuum. The HRTEM images, EDX pattern, and XRD spectrum of $Pt_{0.5}Ru_{0.5}$−PVP−GNF_H were also measured (see Supporting Information, Figures S3, S4, and S5). For the purpose of comparison, Figure 11 shows the chronoamperometric curves for both Pt and PtRu carbon nanocomposites, that is, PtRu−PVP−GNF_H (upper curve) and Pt−PVP−GNF_H (middle curve), and Pt−AO-GNF_H (lower curve) in a H_2SO_4 (0.5 M)−CH_3OH (1 M) aqueous solution at a constant potential of 0.6 V_{NHE}. At the beginning, the current of the $Pt_{0.5}Ru_{0.5}$−PVP−GNF_H nanocomposite is ~50% higher but decays more rapidly than that of the Pt−PVP−GNF_H nanocomposite. This might be because of the easy deactivation of the Pt (110) crystalline phase (the most abundant Pt crystalline phase present in the PtRu alloy nanoparticles[41]) on PtRu nanoparticles at an early time scale by the CO_{ads} species generated during the methanol oxidation processes. The Ru atom in the PtRu alloy could promote oxidation of the surface-absorbed CO_{abs} to CO_2,

leading to activity recovery of the Pt catalyst.[44] When the accumulation and promotion of oxidation of CO-like species reach a balance, the observed electrocatalytic current for PtRu alloy reaches a stable stage. Overall, because of the presence of Ru atoms (and thus the promoted oxidation of CO-like species), the PtRu alloy has a ~46% or ~250% larger electrocatalytic current than the Pt−PVP−GNF_H or the Pt−AO-GNF_H nanocomposites after 5 h continuous electrocatalysis at a 0.6 V applied voltage. Note that the electrocatalytic current was normalized to the weight of PtRu alloy, not to the weight of Pt alone. If normalized to the weight of Pt in the PtRu alloy, the above values will be doubled. Figure 11 also shows the long-term current vs time stabilities of the Pt−AO-GNF_H as well as the Pt−PVP−GNF_H nanocomposites. Basically, the long-term stability of these two nanocomposites are very similar, except that the Pt−PVP−GNF_H has much higher catalytic current/activity, which is attributed to its much higher catalyst surface and electrical conductivity, as compared to the Pt−AO-GNF_H nanocomposite.

Conclusion

We have developed a new, mild PVP surface grafting process and systematically compared the effects of surface functionalization processes on the structural damage, loading, dispersion, and performance of seven different Pt−/PtRu−carbon nanocomposites toward electrocatalytic oxidation of methanol. All spectroscopic data, including TEM, XRD, XPS, and Raman, indicate that the PVP modification process is superior to the conventional acid oxidation method, causing much less structural damage, resulting in a higher density of surface functional groups, smaller average sizes, and better dispersion of metal nanoparticles on carbon supports. The electrical conductivity measurements show that $MWCNT_{arc}$ has higher electrical conductivity (~31 S cm^{-1}) than Vulcan XC-72R carbon black (7.6 S cm^{-1}), GNF_H (14.2 S cm^{-1}), and $MWCNT_{CVD}$ (13.6 S cm^{-1}). Surface modification leads to decrease in the electrical conductivities for all carbon nanomaterials. PVP-modified carbon nanomaterials, however, retain higher electrical conductivities than the corresponding acid-oxidized nanomaterials. The DMFC electrocatalytic activities of seven Pt−carbon nanocomposites have the following sequence: Pt−PVP−GNF_H > Pt−PVP−$MWCNT_{arc}$ > Pt−AO-$MWCNT_{arc}$ > Pt−PVP−$MWCNT_{CVD}$ > Pt−AO-$MWCNT_{CVD}$ > Pt−SC-72R > Pt−AO-GNF_H, with the Pt−PVP−GNF_H nanocomposite having ~270% better electrocatalytic activity than that of the Pt−Vulcan XC-72R nanocomposite. All Pt−PVP−carbon nanocomposites exhibit 17−463% higher DMFC activities than the corresponding AO-carbon nanocomposites. Amazingly, a change of the surface modification process reverses the worst DMFC performance of the Pt−AO-GNF_H nanocomposite to the best for the Pt−PVP−GNF_H nanocomposites. The results highlight the importance of the surface modification process. The key factor reversing the DMFC performance of surface-modified GNF_H nanocomposites is the electrical conductivity of the carbon supports. Overall, the electric conductivity and surface area of supporting carbon nanomaterials, and the EAS of metal catalysts, are identified to be three key factors determining the overall electrocatalytic performance of the final Pt−carbon nanocomposites. The problems of "sulfur poisoning" and the "poor mass transport in micropores" are the two lethal drawbacks for the Vulcan XC-72R carbon black, which has the largest surface area among all. GNF_H has a larger surface area (158.4 m^2/g) but much weaker chemical tolerance toward a harsh acid oxidation method than does MWCNT. By choosing the mild PVP surface grafting process (to avoid the structural damage and to retain electrical conductivity), GNF_H could become one of the best carbon supports in DMFC applications. Finally, we also demonstrated that the PtRu−PVP−GNF_H could be prepared via the PVP grafting process and shows ~50% higher DMFC activity than the best Pt−PVP−GNF_H nanocomposite. Overall, the newly developed PVP surface functionalization process is a general method for mild surface modification of carbon nanomaterials for applications in catalysis and fuel cells.

Acknowledgment. The authors are grateful to the National Science Council, Taiwan, for the financial support.

Supporting Information Available: FT-IR spectra of acid-oxidized and PVP-grafted carbon materials, TEM images of several Pt−/PtRu−carbon nanocomposites, EDX and XRD spectra of PtRu−PVP−GNF_H nanocomposite. These materials are available free of charge via the Internet at http://pubs.acs.org.

JA072367A

(44) Ticianelli, E.; Beery, J. G.; Paffett, M. T.; Gottesfeld, S. *J. Electroanal. Chem.* **1989**, *258*, 61.